

Communication

Electrochemical Detection of Furaltadone Antibiotic Drug by the Rare Earth Metal Tungstate Decorated Screen Printed Carbon Electrode

Sivaramakrishnan Vinothini ^{1,2}, Te-Wei Chiu ^{1,2,*}  and Subramanian Sakthinathan ^{1,2}

¹ Department of Materials and Mineral Resources Engineering, National Taipei University of Technology, No. 1, Section 3, Zhongxiao E. Rd, Taipei 106, Taiwan; vinodhinisakthinath@gmail.com (S.V.); sakthinathan1988@gmail.com (S.S.)

² Institute of Materials Science and Engineering, National Taipei University of Technology, No. 1, Section 3, Zhongxiao E. Rd, Taipei 106, Taiwan

* Correspondence: tewei@ntut.edu.tw; Tel.: +886-2-2771-2171 (ext. 2742)

Abstract: Furaltadone (FLD) is an antibiotic drug that is widely treated for coccidiosis, intestinal infection, and turkey blackhead. Moreover, excessive use of FLD may have some negative consequences for humans and domestic animals. Therefore, practical, sensitive, selective, and facile detection of FLD is still needed. In this exploration, a $\text{Eu}_2(\text{WO}_4)_3$ -nanoparticles-modified screen-printed carbon electrode was developed for the low-level detection of FLD. Hydrothermal techniques were used effectively to prepare the $\text{Eu}_2(\text{WO}_4)_3$ complex. Scanning electron microscopy and X-ray diffraction investigations were used to confirm the $\text{Eu}_2(\text{WO}_4)_3$. The results revealed that the $\text{Eu}_2(\text{WO}_4)_3$ was well formed, crystalline, and uniformly distributed. Furthermore, the electrochemical behavior of the SPCE/ $\text{Eu}_2(\text{WO}_4)_3$ electrode was examined by differential pulse voltammetry and cyclic voltammetry studies. The SPCE/ $\text{Eu}_2(\text{WO}_4)_3$ electrode demonstrated improved electrocatalytic activity in the detection of FLD with a detection limit of 97 μM ($S/N = 3$), linear range of 10 nM to 300 μM , and sensitivity of 2.1335 $\mu\text{A } \mu\text{M}^{-1} \text{ cm}^{-2}$. The SPCE/ $\text{Eu}_2(\text{WO}_4)_3$ electrode detected FLD in the presence of 500-fold excess concentrations of other interfering pollutant ions. The practical feasibility of the SPCE/ $\text{Eu}_2(\text{WO}_4)_3$ electrode was tested on different antibiotic medicines and showed adequate recovery. Moreover, the SPCE/ $\text{Eu}_2(\text{WO}_4)_3$ electrode shows appreciable repeatability, high stability, and reproducibility.

Keywords: $\text{Eu}_2(\text{WO}_4)_3$; screen printed carbon electrode; furaltadone; real sample analysis; antibiotics medicine



Citation: Vinothini, S.; Chiu, T.-W.; Sakthinathan, S. Electrochemical Detection of Furaltadone Antibiotic Drug by the Rare Earth Metal Tungstate Decorated Screen Printed Carbon Electrode. *Technologies* **2023**, *11*, 105. <https://doi.org/10.3390/technologies11040105>

Academic Editors: Dennis Douroumis and Nam-Trung Nguyen

Received: 31 May 2023

Revised: 19 July 2023

Accepted: 2 August 2023

Published: 6 August 2023



Copyright: © 2023 by the authors. Licensee MDPI, Basel, Switzerland. This article is an open access article distributed under the terms and conditions of the Creative Commons Attribution (CC BY) license (<https://creativecommons.org/licenses/by/4.0/>).

1. Introduction

Furaltadone (FLT) is a nitrofurantoin derivative in the family of synthetic antimicrobials, antibiotics, and chemotherapeutic agents. FLT antibiotics are widely used to treat coccidiosis, intestinal infections, and turkey blackhead [1,2]. However, excessive usage of FLT can cause side effects. Generally, FLT is found in animal products such as seafood, fish, poultry, shrimp, and cattle. FLT is commonly applied as a feed additive to promote growth evolution, bacterial infections, prevents protozoa in bee colonies, livestock, and aquaculture [3]. FLT is an antibiotic and a synthetic chemotherapeutic drug also found in poultry, fish, cattle, and shrimp. FLT and its derivatives have been linked to carcinogenic and mutagenic effects [4]. Therefore, many countries, such as the United States of America, Australia, China, the Philippines, Thailand, and Brazil, have banned FLT in food production and antibiotics medicine [5]. The European Union forbidden FLT use in the production of animal food and aquaculture products. Moreover, the World Health Organization (WHO) set the FLT residue level at 1 g/kg, and the Chinese Ministry of Agriculture classified an acceptable level of FLD in aquatic foods as 0.25 $\mu\text{g kg}^{-1}$ [6]. Hence, the need to develop

a technique to identify the quantity of FLT in foods and animal products is necessary. Furthermore, the persistent release of FLT into the green environment as a result of hospital or industrial disposal produces chronic toxicity in all living species. As a result, many academics and industrialists are concerned about the mineralization of FLT from industry. In addition to that, FLT can be metabolized rapidly in the human body, which contributes to its related diseases [7]. Therefore, a practical, facile, and sensitive technique for the detection of the aforementioned hazards of FLT is high importance [8,9]. It is even more important and difficult to prepare interface materials for the electrochemical detection of furaltadone because FLD has a short half-life, is unstable, easily breaks down into its metabolite and 3-amino-5-morpholinomethyl-2-oxazolidinone [10–13].

Different detection methods have been reported to determine the level of antibiotic drugs. They include liquid chromatography-UV photodiode array detection, high-performance liquid chromatography (HPLC), spectrophotometry, liquid chromatography-mass spectrometry (LCMS), fluorimetry, and enzyme-linked immunosorbent sensors [14]. The significant disadvantages of using these traditional methods are that they have a longer duration until results, entail high costs, need well-qualified technicians to operate, are sophisticated instrumentation, and require critical sample preparation [15]. To overcome these issues, the electrochemical method was used due to its low cost, rapid response, simplicity, reliability, excellent sensitivity, marvelous selectivity, and better reproducibility. In comparison to other methodologies, the electrochemical method is the most effective tool for analyzing FTD [16].

Rare earth metals have been used in metallurgy, optics, electrocatalysis, magnetic and other fields due to their unique properties. Rare earth metals have excellent properties and are widely applied in laser materials, superconductors, batteries, solar cells, supercapacitors, and electrochemical sensors due to their different electrical properties [17,18]. Rare earth elements are also fascinating due to the unusual features that result from their electrical structure. These qualities can be attributed to the contraction of 4f orbitals, which are altered by the 5s and 5p shells and have a significant impact on the chemical properties. These elements are very interesting for their excellent mechanical, thermal, chemical, optical, and electrical properties that can be applied in photonic devices and catalysts [19,20].

The rare earth element tungstate has the general formula $RE_2(WO_4)_3$, where R stands for a rare earth element ($RE = La^{2+}, Ce^{2+}, Pr^{2+}, Er^{2+}$, etc.). Moreover, tungstate has demonstrated remarkable performance in ionic conductors, solid-state lasers, and catalysis. It is regarded as an ideal host material for doped RE ions due to the unique characteristics of the WO_4^{2-} groups. $Eu_2(WO_4)_3$ is a critical member of the tungstate family due to its excellent ionic characteristics and strong electrical conductivity [21]. $Eu_2(WO_4)_3$ has very good catalytic properties in addition to its synergistic properties. Among all these tungstates, $Eu_2(WO_4)_3$ is important for its high thermal stability, optical, electrical properties, supercapacitors, and Li-ion battery. $Eu_2(WO_4)_3$ tends to form mixed phases by the solid-state preparation processes in high calcination temperatures. For the synthesis of rare earth metal tungstate, various methods have been developed, including sol-gel processing, solid-state reaction, microemulsion, molten-salt-assisted crystallization, and hydrothermal reaction. Surprisingly, one of the better alternative methods for nanomaterial synthesis is the hydrothermal method [20–22].

In this paper, we describe the hydrothermal synthesis of $Eu_2(WO_4)_3$ as a simple, flexible, and straightforward method. In addition, the electrochemical performance of as-prepared $Eu_2(WO_4)_3$ nanoparticles was evaluated using different characterization methods. The synthesized $Eu_2(WO_4)_3$ was applied as a sensor material for the determination of FTD. The electrocatalytic behavior of the SPCE/ $Eu_2(WO_4)_3$ electrode used for FTD detection was very high compared to that of the unmodified SPCE. Furthermore, we find that the SPCE/ $Eu_2(WO_4)_3$ had excellent electrochemical activity for FTD detection and could be successfully applied to real sample analysis. The developed SPCE/ $Eu_2(WO_4)_3$ electrode demonstrated high sensitivity, selectivity, and the lowest detection limit for FTD detection. These electrochemical detections have multiple benefits, including ease of use, excellent

selectivity, high sensitivity, low cost, and quick response times. At the same time, these detection techniques have several downsides, including the costly raw materials of the electrode, longer preparation time, and environmental pollution during the preparation of the electrode material. Additionally, the electrodes must be prepared using the right procedures to maintain consistent performance. The prepared SPCE/Eu₂(WO₄)₃ electrochemical sensor also has outstanding electrochemical sensing capabilities for the detection of FT and demonstrates its potential catalytic sensing use in pharmaceutical samples.

2. Materials and Methods

Screen-printed carbon electrodes (0.08 cm²) were acquired from Zensor R&D Co., Ltd., Taipei, Taiwan. Europium (III) chloride (EuCl₃·6H₂O), methanol, sodium tungstate dihydrate (Na₂WO₄·2H₂O), furmethanol (C₁₃H₁₆N₄O₆), and all other chemicals were received from Sigma-Aldrich Chemical Company, Taipei, Taiwan. Furthermore, sulfuric acid (H₂SO₄) chemical, and hydrochloric acid (HCl) chemicals were obtained from Merck Chemical Company. The supporting phosphate-buffered solution (PBS) electrolyte was made by using 0.05 mol L⁻¹ of Na₂HPO₄ and 0.05 mol L⁻¹ of monosodium phosphate (NaH₂PO₄). These FTD standard solutions were prepared by dissolving the appropriate amount of dimethylformamide (DMF) with FTD. All chemicals were made by analytical-reagent grade chemicals without further purification. All solutions were made using double distilled water, PBS (pH 7) was used to make a stock solution of furaltadone, and nitrogen purging was used to simultaneously deoxygenate the electrolyte.

The electrochemical evaluation by differential pulse voltammetry and cyclic voltammetry studies was conducted on CHI 1211B workstations, respectively. The CHI 1211B workstations were linked to a standard three-electrode cell that included an Ag/AgCl electrode as a reference electrode, an SPCE as a working electrode, and a Pt needle was used as counter electrodes, respectively. All the electrochemical studies were conducted at normal laboratory temperatures. Field emission scanning electron microscopy (FESEMEDX, JEOL JSM-7610F, Tokyo, Japan, and Hitachi Regulus 8100) combined with energy-dispersive X-ray spectroscopy was used to identify and assess the surface morphology with the elemental arrangement. Micro Raman Spectrum (Uni Nano Tech Co., Ltd., ACRON, Yongin, Republic of Korea) with an excitation source of 532 nm and a resolution of 1 m was used to identify the Raman spectra. An X-ray diffractometer (D2 Phaser, Bruker, Billerica, MA, USA) was used to study spectra under CuKα radiation (λ = 1.5418 Å).

2.1. Preparation of Eu₂(WO₄)₃ Nanoparticles by Hydrothermal Methods

Eu₂(WO₄)₃ nanoparticles were prepared according to previous reports with slight modification [18,20,22,23]. A hydrothermal process was used to create Eu₂(WO₄)₃ nanoparticles. Under the ambient condition, analytical grade Eu(NO₃)₃·6H₂O and Na₂WO₄·2H₂O reagent solutions were continually mixed, and the suspension was transported to an autoclave and thermally treated at 180 °C in the oven for 12 h. After the hydrothermal process, white color fine powder was obtained and separated by centrifuging with water, washed with ethanol/water mixture, and finally dried in the oven. The resulting white powder was washed with deionized water and pure ethanol. The precipitate was dried in a hot air oven set to 60 °C. The prepared materials were crushed into white fine powders using a Hitech Agate mortar. These materials were calcined at 600 °C for 5 h in a muffle furnace to create crystalline Eu₂(WO₄)₃ nanoparticles.

2.2. Fabrication of SPCE/Eu₂(WO₄)₃ Modified Electrode by Simple Drop-Casting Methods

The SPCE was cleaned with ethanol and water before being dried at room temperature to remove the weakly adsorbed contaminants. The ASPCE was prepared using previously described methods [24]. In detail, SPCE was initially cleaned with ethanol/water by sonication to remove the adsorbed materials on the ASPCE surface. Then, the cleaned SPCE was shifted into an electrochemical cell containing PBS (pH 7)/KCl electrolytes mixture, followed by the applied potential 0 to 2.0 V up to 20 cycles for ASPCE preparation. After

the ASPCE preparation, 2 mg of prepared $\text{Eu}_2(\text{WO}_4)_3$ nanoparticles were dispersed in 200 μL of DD water and kept in an ultra-sonication bath for 15 min to form a homogeneous white color suspension. Later, 8 μL of $\text{Eu}_2(\text{WO}_4)_3$ nanoparticles were coated on the surface of the activated SPCE and dried in a hot oven at 50 $^\circ\text{C}$. The obtained $\text{Eu}_2(\text{WO}_4)_3/\text{SPCE}$ electrode was used for additional electrochemical studies.

3. Characterization Studies of Materials

XRD, SEM, and EDX Studies

The structural morphology and crystalline structure arrangement of the as-prepared $\text{Eu}_2(\text{WO}_4)_3$ nanoparticles are shown in Figure 1. Figure 1A shows that the XRD diffraction pattern of $\text{Eu}_2(\text{WO}_4)_3$ nanoparticles displayed a monoclinic phase. The $\text{Eu}_2(\text{WO}_4)_3$ had diffraction peaks at 28.55 $^\circ$, 30.8 $^\circ$, 34.12 $^\circ$, 46.95 $^\circ$ and 57.74 $^\circ$ for the 101, 102, 111, 112, and 120 planes, respectively. This diffraction is concordant with the standard PDF file (PDF#22-0287) of the $\text{Eu}_2(\text{WO}_4)_3$ monoclinic phase [25]. The results indicate a good formation of $\text{Eu}_2(\text{WO}_4)_3$ nanoparticles.

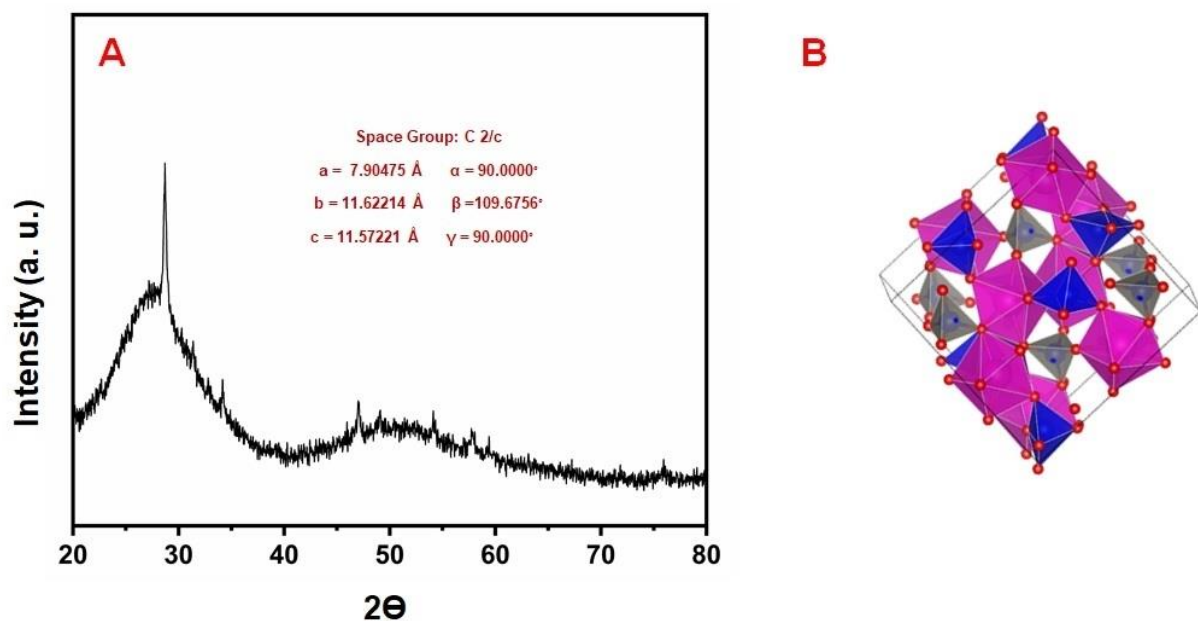


Figure 1. (A) XRD spectra of $\text{Eu}_2(\text{WO}_4)_3$ and (B) crystal structure of $\text{Eu}_2(\text{WO}_4)_3$.

Figure 2A,B shows the FESEM structural images of the $\text{Eu}_2(\text{WO}_4)_3$ nanoparticles showing the coral shape structure and the particles typical size of approximately 300 nm. Figure 2C shows the EDX spectra and elemental mapping results used to study the chemical composition of the $\text{Eu}_2(\text{WO}_4)_3$ nanoparticles. Additionally, the elemental mapping results of $\text{Eu}_2(\text{WO}_4)_3$ nanoparticles revealed the presence of europium (Figure 2D), tungstate (Figure 2E), and oxygen (Figure 2F). Furthermore, Figure 2G exhibits the EDX spectra of $\text{Eu}_2(\text{WO}_4)_3$ nanoparticles, showing the homogeneously distributed elements observed, such as europium (Eu), tungstate (W), and oxygen (O).

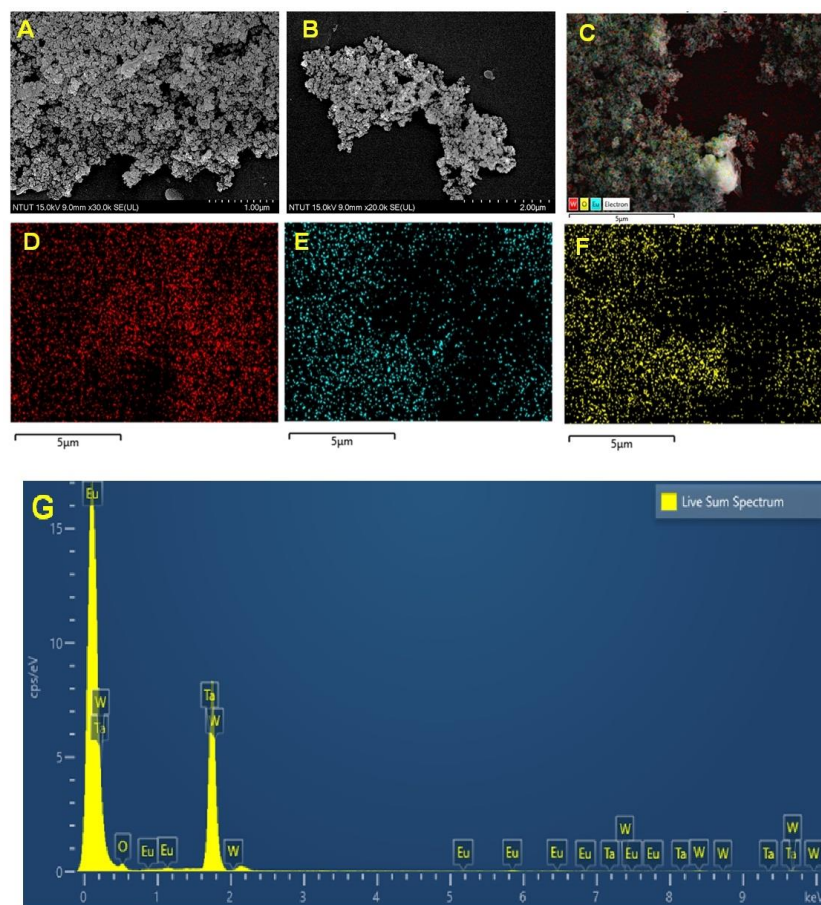


Figure 2. (A,B) FESEM image of $\text{Eu}_2(\text{WO}_4)_3$. (C) $\text{Eu}_2(\text{WO}_4)_3$ elemental mapping results of (D) Eu, (E) W, and (F) O. (G) shows the EDX spectra of $\text{Eu}_2(\text{WO}_4)_3$.

4. Electrochemical Studies of FTD on the ASPCE/ $\text{Eu}_2(\text{WO}_4)_3$ Electrode

4.1. Effects of Different Films and Effects of Different Concentrations

The electrocatalytic activity of FLD at different modified electrodes was identified using CV at a scan rate of 50 mVs^{-1} in the presence of $100 \mu\text{M}$ of FLD in 0.05 M PBS ($\text{pH} = 7$). Figure 3A exhibits the electrochemical detection response of FLD at the SPCE, ASPCE, and ASPCE/ $\text{Eu}_2(\text{WO}_4)_3$ electrodes. The SPCE electrode had a low peak current of $73 \mu\text{A}$ for the addition of $100 \mu\text{M}$ of FLD. The ASPCE electrode exhibited the detection response of $80 \mu\text{A}$ at the potential of -0.4 V . The SPCE/ $\text{Eu}_2(\text{WO}_4)_3$ electrode exhibited a FLD detection peak current response of $-106.3 \mu\text{A}$. The SPCE/ $\text{Eu}_2(\text{WO}_4)_3$ electrode reached the FLD detection peak current response of $-155.5 \mu\text{A}$, indicating that the reduction potential of FLD was higher than those of the SPCE, ASPCE, and SPCE/ $\text{Eu}_2(\text{WO}_4)_3$ electrodes. However, no characteristic peak was observed for ASPCE/ $\text{Eu}_2(\text{WO}_4)_3$ in the absence of $100 \mu\text{M}$ FLD (Figure 3B). This aforementioned result indicates the excellent catalytic behavior of the ASPCE/ $\text{Eu}_2(\text{WO}_4)_3$ electrode towards FLD. This suggests that the $\text{Eu}_2(\text{WO}_4)_3$ coated on the ASPCE can enhance the oxidation signal and electron transfer capability of the ASPCE/ $\text{Eu}_2(\text{WO}_4)_3$ electrode.

Electrochemical detection mechanisms of FLD contain a nitro group (R-NO_2), which is electrochemically reduced to form a hydroxylamine group (R-NHOH) with an equal number of electrons ($+4e^-$) and protons ($+4\text{H}^+$) in the electron transfer process (Scheme 1). This irreversible reduction process of FLD at the surface of the ASPCE/ $\text{Eu}_2(\text{WO}_4)_3$ electrode is indicated by the electrochemical reduction of FLD. A weak redox peak indicates O1 for oxidation and R2 for reduction at potentials of $+0.15 \text{ V}$ and 0.07 V , respectively. This electrochemical process turns hydroxylamine (NH_2OH) into a nitroso derivative by the two-electron and two-proton transfer reaction. The R1 peak signal observed for the reduction peak current (R1) of FLD is significantly larger than the redox couple. The ASPCE/ $\text{Eu}_2(\text{WO}_4)_3$

demonstrated outstanding electrochemical performance for FLD sensing due to the highly specialized surface area, which promotes fast electron conductivity. The Randles Sevcik equation and the hexacyanoferrate system ($K_3[Fe(CN)_6]^{3-/4-}$) were used to determine the modified electrode active surface area. The ASPCE (0.052 cm^2) and SPCE/ $Eu_2(WO_4)_3$ (0.135 cm^2) electrodes have much lower active surface areas than the ASPCE/ $Eu_2(WO_4)_3$ (0.191 cm^2) electrodes. Hence, the active surface area of the ASPCE/ $Eu_2(WO_4)_3$ electrode is one of the reasons for the high electrochemical activity toward the detection of FLD.

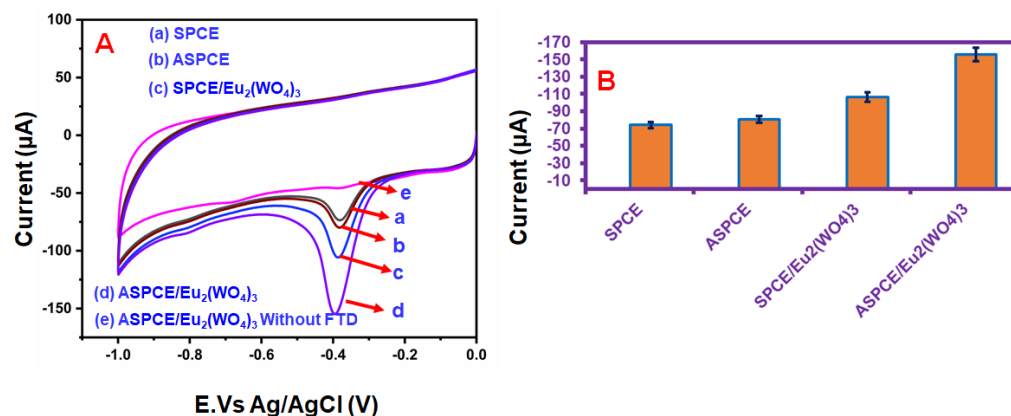
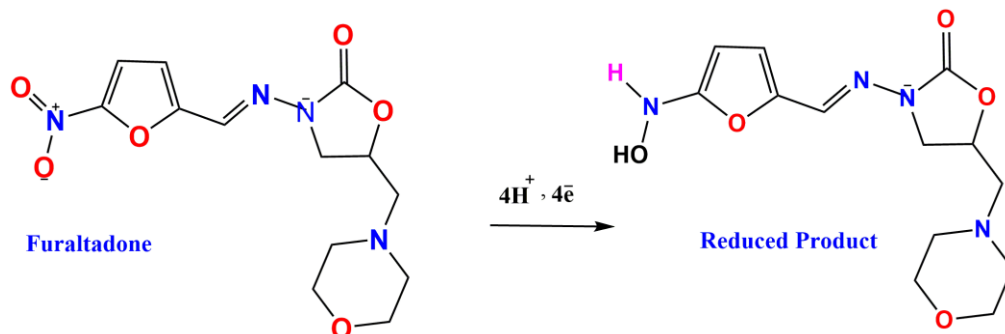


Figure 3. (A) CV response of (a) SPCE, (b) ASPCE, (c) SPCE/ $Eu_2(WO_4)_3$, (d) ASPCE/ $Eu_2(WO_4)_3$ electrodes in 0.05 M PBS (pH 7) with 100 μM of FTD and (e) ASPCE/ $Eu_2(WO_4)_3$ in absence of FTD. (B) Bar diagram of the peak current of SPCE, ASPCE, SPCE/ $Eu_2(WO_4)_3$, and ASPCE/ $Eu_2(WO_4)_3$ electrodes.



Scheme 1. Possible electrochemical detection (reduction) mechanism of FLD.

In addition, Figure 4A shows the CV performances of different concentrations (100–700 μM) of FLD in deoxygenated 0.05 M PBS. The FLD reduction peak currents linearly increased with increases in the concentration of FLD (Figure 4B). The corresponding linear regression equation was obtained as $IP = 75.58v^{1/2} (\text{Vs}^{-1})^{1/2} + 10.60$ with $R^2 = 0.998$. Therefore, an excellent and fast electron transfer was observed at the ASPCE/ $Eu_2(WO_4)_3$ surface due to the good electrostatic interaction between the ASPCE and $Eu_2(WO_4)_3$, which increased the higher electron flow rate and surface area of the composite matrix.

4.2. Effect of Different Scan Rates and Effect of Different pH Studies

Figure 5A reveals a noteworthy CV curve obtained at the ASPCE/ $Eu_2(WO_4)_3$ electrode for the different scan rates in 100 μM of FLD containing PBS (pH 7). These results indicated that the FLD reduction peak current response linearly increased with increases in scan rates from 10 to 160 mVs^{-1} . Figure 5B shows the related peak current (IP) vs. scan rate plot and the corresponding linear regression equation was obtained as $IP = 75.58v^{1/2} (\text{Vs}^{-1})^{1/2} + 10.60$ with $R^2 = 0.998$.

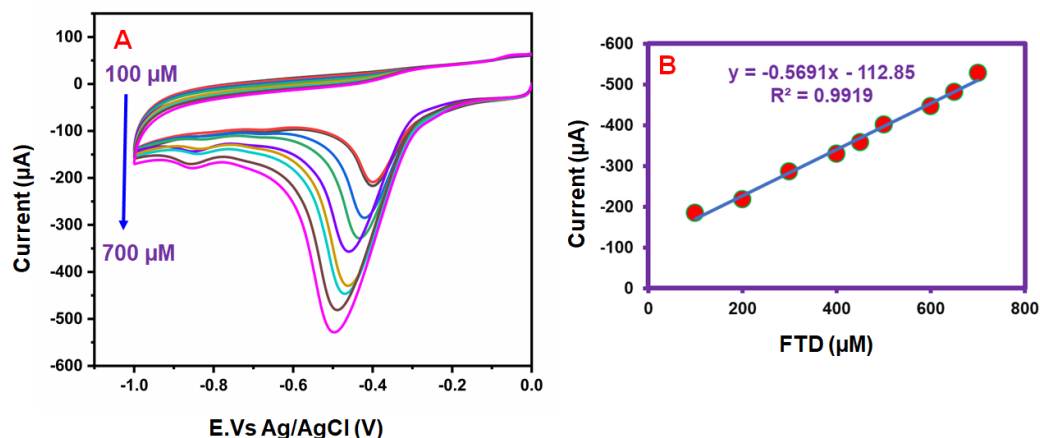


Figure 4. (A) Cyclic voltammogram of ASPCE/Eu₂(WO₄)₃ in 0.05 M PBS (pH 7) containing different concentrations of FLD at a scan rate of 50 mVs⁻¹ (Different colors are mentioned for different concentration of FLD peak currents). (B) Correspondences to the calibration plot for FLD concentrations (100–700 µM) vs. peak current.

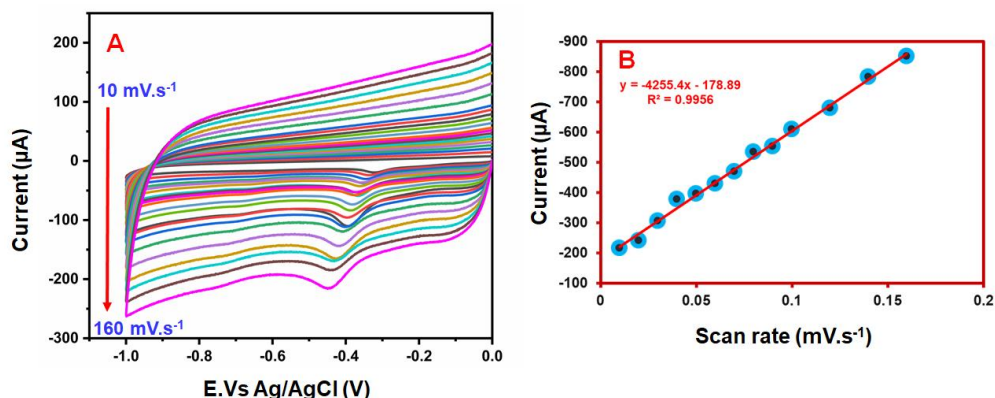


Figure 5. (A) Effect of different scan rates at ASPCE/Eu₂(WO₄)₃ electrode on the reduction of FLD (100 µM) present in PBS (pH 7) (Different colors are mentioned for different scan rates peak currents). (B) Calibration graph for the reduction of FLD between scan rate and peak current.

This result shows that the reduction of FLD is a surface-controlled process over the ASPCE/Eu₂(WO₄)₃. Moreover, with an increasing scan rate, the electrocatalytic reduction of FLD at an ASPCE/Eu₂(WO₄)₃ electrode peak shifted to a negative potential. The electron transfer coefficient and the number of electrons transferred are involved in the rate-determining step. In addition, the number of electrons transferred involved in the reduction of FLD can be calculated by the surface-controlled reaction. This result indicates that the FLD reduction leads to the final product, and it is in good accordance with the previously published results. The overall reduction reaction can be expressed by the electrocatalytic reduction of FLD at the ASPCE/Eu₂(WO₄)₃ electrode as a two-electron transfer reaction.

The CV studies showed the influence of electrolyte pH on the ASPCE/Eu₂(WO₄)₃ electrode for the detection of FTD. The CV experiment was recorded at ASPCE/Eu₂(WO₄)₃ electrodes at pH levels of 3 to 11 during the electrocatalytic reduction of 100 µM of FTD. As mentioned in Figure 6A, the reduction peak current of FTD increased as electrolyte pH values rose from 3 to 7, and afterward, it decrease at pH levels of 9 to 11 (Figure 6B). This result exhibited that, at lower pH, the FTD molecules are unstable and easily converted into reduced products. In the same experiment at higher pHs, proton deficiency occurred in the electrolytes. However, at pH 7, the electrochemical sensor exhibited higher electrocatalytic performance toward the detection of FTD. Therefore, in this work, we chose pH 7 for further electrochemical studies.

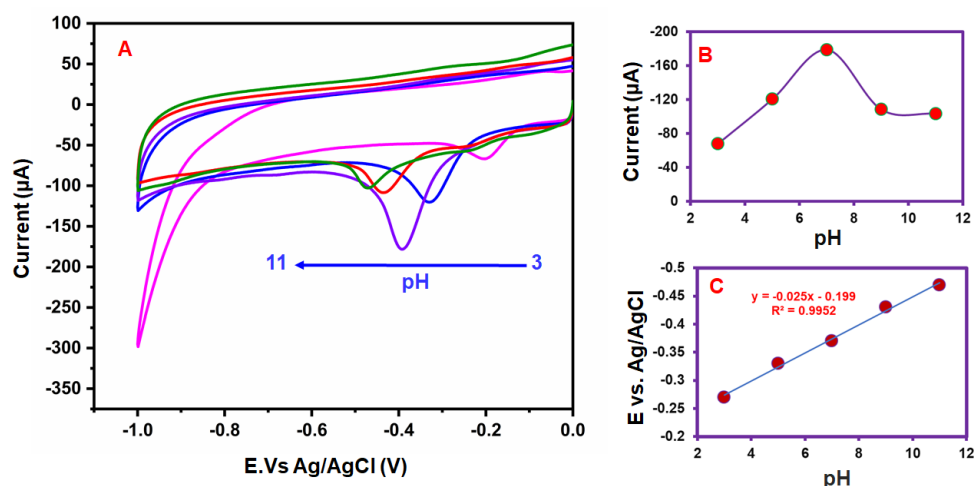


Figure 6. (A) Cyclic voltammetry performance of FTD reduction at different pH from 5 to 11. (B) FTD reduction peak current vs. pH (Different colors are mentioned for different pH peak currents). (C) Effects of pH on the FTD reduction peak potential vs. pH.

4.3. DPV Studies for Detection of FLD

DPV technique is an overall more sensitive and unique procedure than other voltammetry methods. For this reason, we used these techniques for the limit of detection, sensitivity and linear limit identification. Figure 7A revealed DPV responses of FLD reduction on ASPCE/Eu₂(WO₄)₃ in 0.05 M PB solution containing different concentrations of FLD addition (0.1–450 µM). The reduction peak current was expanded with increasing the concentration of FLD. Figure 7B indicates the linear calibration plot amid the peak current (*I_p*) and FLD concentration. The linear concentration ranges of the ASPCE/Eu₂(WO₄)₃ electrode were 0.1–125 µM and the limit of detection (LOD) was 7.4 nM. Additionally, the sensitivity of the ASPCE/Eu₂(WO₄)₃ electrode was fixed at about 4.1084 µA µM⁻¹ cm⁻², which is an excessive value compared with that of the other electrodes. In consequence, the results demonstrate that the ASPCE/Eu₂(WO₄)₃ electrode exhibited superior detection of FLD due to the higher electron transfer rate and good-catalytic behavior of the Eu₂(WO₄)₃. Furthermore, the surface nature of ASPCE distributed a strong interaction between the ASPCE and Eu₂(WO₄)₃. For that reason, the ASPCE/Eu₂(WO₄)₃ modified electrode was used as a predominant electrode material for the electrochemical detection of FLD. The acquired performance results are compared with previously published FLD sensors and mentioned in Table 1. Moreover, the electrochemical detection of the carbendazim at the ASPCE/Eu₂(WO₄)₃ electrode was lower than that of the other reported electrodes and methods, such as the FeVO/p-rGO NCs electrode [LOD = 138 nM] [26], AOZ/AMOZ electrode [LOD = 10 µg kg⁻¹] [27], LC-MS/MSc method [LOD = 0.5 µg kg⁻¹] [28], ELISA method [LOD = 0.3 µg kg⁻¹] [29], and LC-MS/MS method [LOD = 0.2 µg/kg] [30]. According to the comparison table, the ASPCE/Eu₂(WO₄)₃ electrode had good selectivity, a wide linear range, and a low LOD. Therefore, Eu₂(WO₄)₃ is a promising candidate for the electrochemical detection of FLD due to its higher electron transfer rate.

Table 1. Comparison of the analytical performance of ASPCE/Eu₂(WO₄)₃ electrode with other FTD sensors.

Electrode and Technique	Linear Range	Limit of Detection	References
FeVO/p-rGO NCs	0.584	138 nM	[26]
AOZ/AMOZ	0.05–2.0	10.0 µg kg ⁻¹	[27]
LC-MS/MSc	1–800	0.5 µg kg ⁻¹	[28]
ELISA	0.9–105.3	0.3 µg kg ⁻¹	[29]
LC-MS/MS	0.98–0.99	0.2 µg/kg	[30]
ASPCE/Eu ₂ (WO ₄) ₃	10 nM–300 µM	97 µM	This work

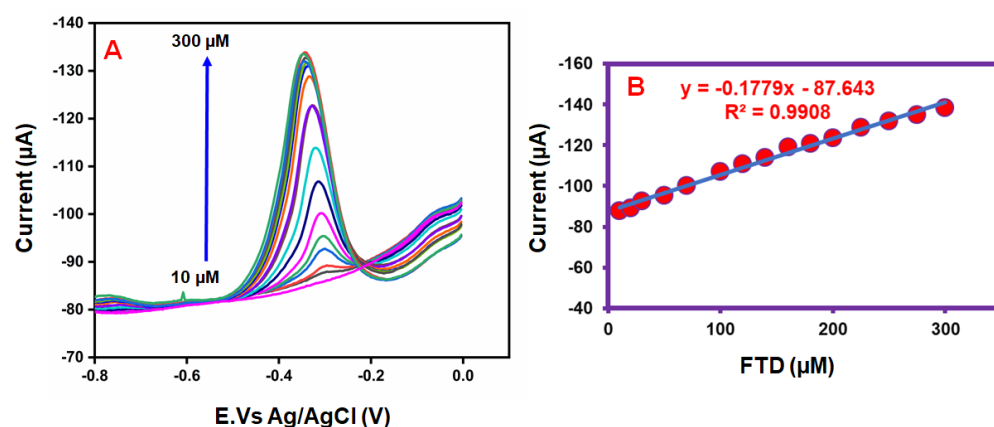


Figure 7. (A) DPV response of ASPCE/Eu₂(WO₄)₃ electrode for different concentrations of FLD in PBS (pH 7) (Different colors are mentioned for different concentration of FLD peak currents). (B) calibration plot of the different concentrations of FLD vs. reduction peak current.

4.4. Repeatability, Cyclic Stability, Reproducibility, and Operational Stability Studies of Eu₂(WO₄)₃ Coated Electrodes

The repeatability and reproducibility performance of the SPCE/Eu₂(WO₄)₃ electrodes were identified by the CV technique. Also, the stability study was conducted in the amperometric technique. The repeatability behavior of three SPCE/Eu₂(WO₄)₃ electrodes was examined to determine the FLD detection. The CV curves showed the same cathodic detection peak currents of FLD with an RSD value of 2.4% (Figure 8A), which indicated that our prepared SPCE/Eu₂(WO₄)₃ electrodes have outstanding repeatability. Reproducibility studies were performed with 50 µM FLD over five different SPCE/Eu₂(WO₄)₃ electrodes consecutively for reproducibility analysis with an RSD value of 2.1% (Figure 8B). Figure 8C shows the cyclic stability responses of the ASPCE/Eu₂(WO₄)₃ electrode in the presence of 100 µM FLD. The CV spectra of the first and 100th cycles had the same peak current values, indicating the excellent cyclic stability of the ASPCE/Eu₂(WO₄)₃ electrode. Furthermore, operational stability studies of the RRDE/Eu₂(WO₄)₃ electrode's response were seen at increases of 100 µM FLD at 50 s intervals, and it preserved 96.5% of its original current up to the 2000 s (Figure 8D). These results prove the excellent operational stability of the RRDE/Eu₂(WO₄)₃ electrode.

4.5. Real Sample Studies of FTD in Antibiotic Medicine

The CV studies approach was utilized to detect FLD in silverzine, sindine, and tetracycline medicine samples with the ASPCE/Eu₂(WO₄)₃ electrode. In real sample analysis studies, the standard addition method was applied for the detection of FLD from antibacterial medicine. Real samples were prepared as follows. Antibacterial medicine was dissolved in water samples and applied for real sample detection. The FLD was then added to the real samples in concentrations of 20, 40, and 60 µM, as shown in Figure 9A–C. Finally, the real sample recovery percentages of the silverzine, sindine, and tetracycline medicine samples ranged from 95–98%, as listed in Table 2. The real sample analysis confirmed that our prepared ASPCE/Eu₂(WO₄)₃ electrode had a good recovery percentage for the detection of FLD in antibacterial medicine samples.

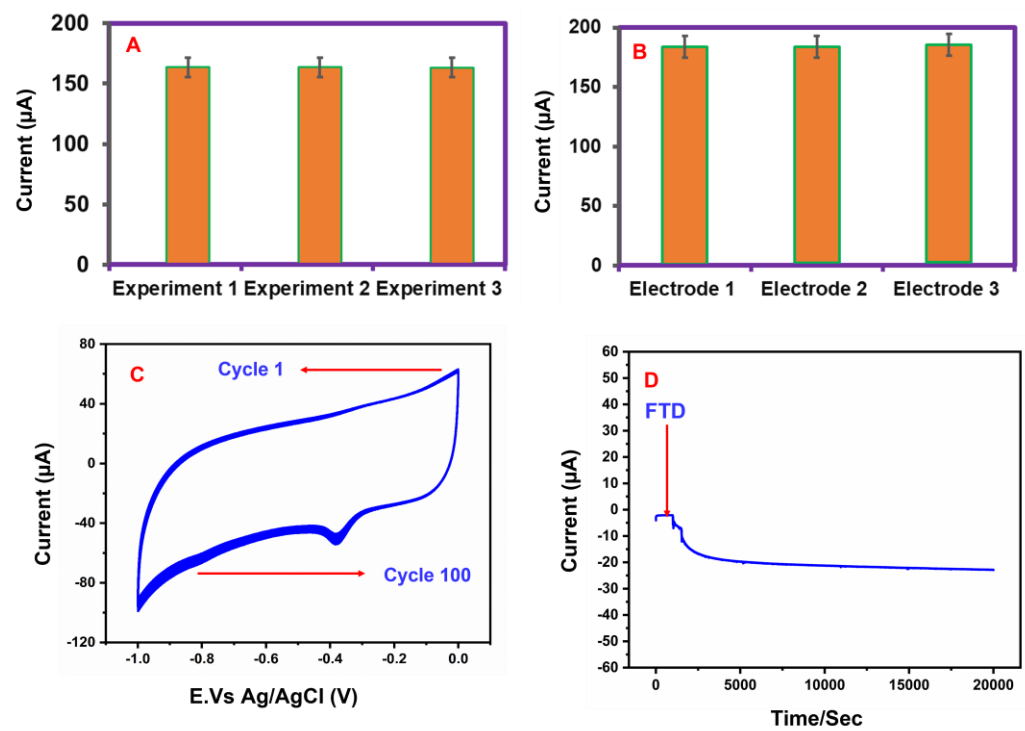


Figure 8. (A) Repeatability study of SPCE/Eu₂(WO₄) electrodes, (B) reproducibility study of SPCE/Eu₂(WO₄) electrodes, (C) cyclic stability study of the RRD/Eu₂(WO₄) electrode, (D) operational stability study of the RRD/Eu₂(WO₄)₃ electrode toward FTD detection in 0.05 M PBS (pH 7) up to 2000 s.

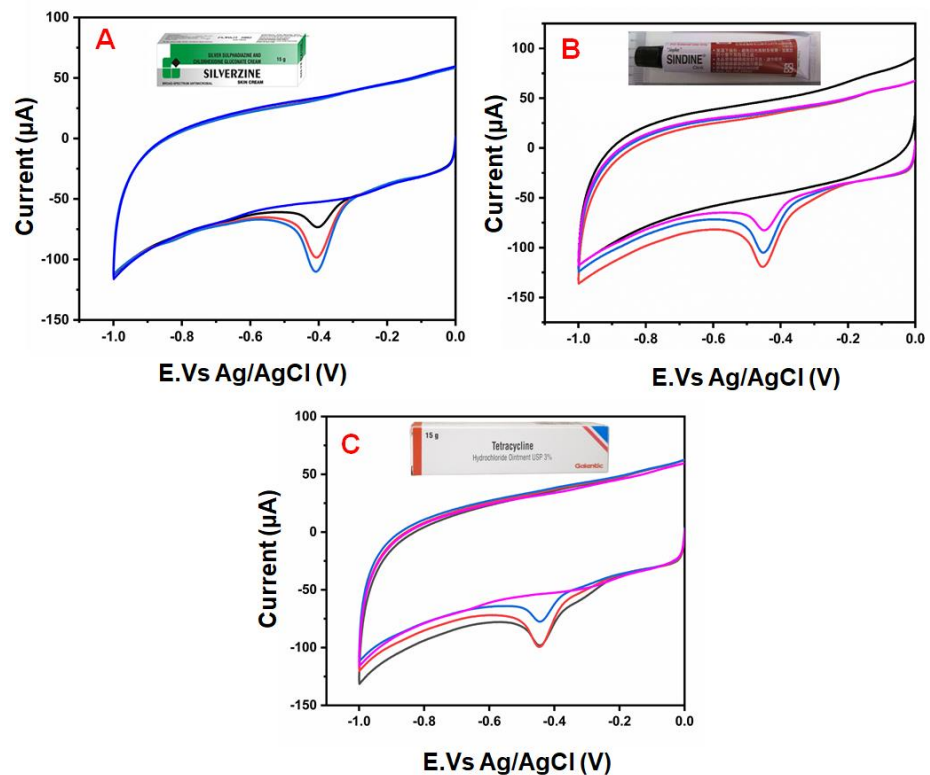


Figure 9. Real sample analysis of FLD in (A) silverzine, (B) sindine, and (C) tetracycline medicine samples.

Table 2. Determination of FTD using different antibiotics medicine by ASPCE/Eu₂(WO₄)₃ electrode.

Real Samples	Added	Found	Recovery (%)
Silverzine medicine	10	9	90
	20	18.5	92.5
	30	29.2	97.3
Sindine medicine	10	8.5	85
	20	19	95
	30	29.4	98
Tetracycline medicine	10	9.3	93
	20	19.3	96.5
	30	29.5	98.3

5. Conclusions

An ASPCE/Eu₂(WO₄)₃ electrode was prepared by non-covalent interaction. The Eu₂(WO₄)₃ complex was identified using different characterization studies. The electrochemical performance of the ASPCE/Eu₂(WO₄)₃ electrode was used to evaluate the cyclic voltammetry, differential pulse voltammetry, and amperometry technique. The ASPCE/Eu₂(WO₄)₃ has excellent electrocatalytic activity concerning the detection of FLD at 0.19 V. Further, the ASPCE/Eu₂(WO₄)₃ electrode had higher electrocatalytic activity towards the detection of FLD due to the high active surface area of Eu₂(WO₄)₃ and fast electrons transport between the ASPCE/Eu₂(WO₄)₃ electrode and FLD. Hence, the proposed ASPCE/Eu₂(WO₄)₃ electrode had good electrocatalytic activity towards the reduction of FLD, with a low detection limit of 97 μM, long linear range of 20–300 μM, and high sensitivity of 2.1335 μA μM⁻¹ cm⁻². Moreover, the ASPCE/Eu₂(WO₄)₃ electrode exhibited good stability, reproducibility, and repeatability. The ASPCE/Eu₂(WO₄)₃ electrode exhibited practical detection in silverzine, sindine, and tetracycline medicine samples with admissible recoveries. Hence, the ASPCE/Eu₂(WO₄)₃ electrode is favorably applicable to the selective, and sensitive detection of FLD.

Author Contributions: Conceptualization, S.V. and S.S.; methodology, S.V.; software, S.V.; validation, S.V., S.S. and T.-W.C.; formal analysis, S.V.; investigation, S.V.; resources, S.V. and S.S.; data curation, S.V.; writing—original draft preparation, S.V.; writing—review and editing, S.V. and S.S.; visualization, S.V.; supervision, T.-W.C.; project administration, T.-W.C.; funding acquisition, T.-W.C. All authors have read and agreed to the published version of the manuscript.

Funding: This work was supported by the Ministry of Science and Technology (MOST 109–2221-E-027–059, 110–2221-E-027–041, NSTC 111–2221-E-027–104, and NSTC 112–2221-E-027–039).

Institutional Review Board Statement: Not applicable.

Informed Consent Statement: Not applicable.

Data Availability Statement: Data are available on request.

Acknowledgments: The authors thank Abinaya Meenakshi, Functional Oxide Laboratory, National Taipei University of Technology (NTUT), Taiwan, for materials characterization help. The authors appreciate the Precision Research and Analysis Centre of the National Taipei University of Technology (NTUT) for providing the measurement facilities.

Conflicts of Interest: The authors declare no conflict of interest.

References

- Diaz, T.G.; Cabanillas, A.G.; Valenzuela, M.I.A.; Correa, C.A.; Salinas, F. Determination of nitrofurantoin, furazolidone, and furaltadone in milk by high-performance liquid chromatography with electrochemical detection. *J. Chromatogr. A* **1997**, *764*, 243–248. [[CrossRef](#)] [[PubMed](#)]
- Mariappan, K.; Chen, T.W.; Chen, S.M.; Tseng, T.W.; Bian, Y.; Sun, T.T.; Jiang, J.; Yu, J. Fabrication of Hexagonal CuCoO₂ Modified Screen-Printed Carbon Electrode for the Selective Electrochemical Detection of Furaltadone. *Int. J. Electrochem. Sci.* **2022**, *17*, 220644. [[CrossRef](#)]

3. Vasu, D.; Keyan, A.K.; Sakthinathan, S.; Chiu, T.W. Investigation of electrocatalytic and photocatalytic ability of Cu/Ni/TiO₂/MWCNTs Nanocomposites for detection and degradation of antibiotic drug Furaltadone. *Sci. Rep.* **2022**, *12*, 886. [[CrossRef](#)] [[PubMed](#)]
4. Amalraj, A.J.J.; Murthy, U.N.; Fue, W.S. Ultrasensitive electrochemical detection of an antibiotic drug Furaltadone in fish tissue with a ZnO-ZnCo₂O₄ self-assembled nano-heterostructure as an electrode material. *Microchem. J.* **2021**, *169*, 106566. [[CrossRef](#)]
5. Massa, A. Clinical trial of furaltadone, an antibacterial nitrofurantoin. *Br. J. Clin. Pract.* **1961**, *15*, 351–354. [[CrossRef](#)]
6. Khodari, M.; Din, H.S.E.; Mersal, G.A.M. Electroreduction and quantification of furazolidone and furaltadone in different media. *Mikrochim. Acta* **2000**, *135*, 9–17. [[CrossRef](#)]
7. Barbosa, J.; Freitas, A.; Moura, S.; Maria, J.L.M.; Silveira, I.N.; Ramos, F. Detection, accumulation, distribution, and depletion of furaltadone and nifursol residues in poultry muscle, liver, and gizzard. *J. Agric. Food Chem.* **2011**, *59*, 11927–11934. [[CrossRef](#)]
8. Xu, Z.L.; Shen, Y.D.; Sun, Y.M.; Campbell, K.; Tian, Y.X.; Zhang, S.W.; Lei, H.T.; Jiang, Y.M. Novel hapten synthesis for antibody production and development of an enzyme-linked immunosorbent assay for determination of furaltadone metabolite 3-amino-5-morpholinomethyl-2-oxazolidinone (AMOZ). *Talanta* **2013**, *103*, 306–313. [[CrossRef](#)]
9. Jester, E.L.E.; Abraham, A.; Wang, Y.; Steven, K.R.E.S.; Plakas, M. Performance evaluation of commercial ELISA kits for screening of furazolidone and furaltadone residues in fish. *Food Chem.* **2014**, *145*, 593–598. [[CrossRef](#)]
10. Shi, S.; Cao, G.; Chen, Y.; Huang, J.; Tang, Y.; Jiang, J.; Gan, T.; Wan, C.; Wu, C. Facile synthesis of core-shell Co-MOF with hierarchical porosity for enhanced electrochemical detection of furaltadone in aquaculture water. *Anal. Chim. Acta* **2023**, *1263*, 341296. [[CrossRef](#)]
11. Alawi, M.A. Analysis of furazolidone and furaltadone in chicken tissues and eggs using a modified HPLC/ELCD method. *Fresenius Environ. Bull.* **2000**, *9*, 508–514.
12. Balamurugan, K.; Rajakumaran, R.; Chen, S.M.; Karthik, R.; Shim, J.J.; Shafi, P.M. Massive engineering of spinel cobalt tin oxide/tin oxide-based electrocatalyst for the selective voltametric determination of antibiotic drug furaltadone in water samples. *J. Alloys Compd.* **2021**, *882*, 160750. [[CrossRef](#)]
13. Kokulnathan, T.; Wang, T.J.; Ahmed, F.; Alshahrani, T. Synthesis of 3D flower-like zinc-chromium layered double hydroxides: A functional electrode material for furaltadone detection. *Process Saf. Environ. Prot.* **2023**, *176*, 889–897. [[CrossRef](#)]
14. Keyan, A.K.; Sakthinathan, S.; Vasu, D.; Yu, C.L.; Vinothini, S.; Chiu, T.W. Gadolinium molybdate decorated graphitic carbon nitride composite: Highly visualized detection of nitrofurazone in water samples. *RSC Adv.* **2022**, *12*, 34066–34079. [[CrossRef](#)]
15. Keyan, A.K.; Vasu, D.; Sakthinathan, S.; Chiu, T.W.; Lee, Y.H.; Lin, C.C. Facile synthesis of silver-doped copper selenide composite for enhanced electrochemical detection of ecological toxic nitrobenzene. *Electrocatalysis* **2023**, *14*, 448–462. [[CrossRef](#)]
16. Sakthinathan, S.; Keyan, A.K.; Vasu, D.; Vinothini, S.; Nagaraj, K.; Mangesh, V.L.; Chiu, T.W. Graphitic carbon nitride incorporated europium molybdate composite as an enhanced sensing platform for electrochemical detection of carbendazim in agricultural products. *J. Electrochem. Soc.* **2022**, *169*, 127504. [[CrossRef](#)]
17. Enayat, M.J. Controllable fabrication of europium tungstate nanoparticles in the presence of new capping agents and investigation of their photocatalytic properties. *J. Mater. Sci. Mater. Electron.* **2017**, *28*, 16444–16449. [[CrossRef](#)]
18. Nasrabadi, M.R.; Pourmohamadian, V.; Karimi, M.S.; Naderi, H.R.; Karimi, M.A.; Didehban, K.; Ganjali, M.R. Assessment of supercapacitive performance of europium tungstate nanoparticles prepared via hydrothermal method. *J. Mater. Sci. Mater. Electron.* **2017**, *28*, 12391–12398. [[CrossRef](#)]
19. Templeton, D.H.; Zalkin, A. Crystal Structure of Europium Tungstate. *Acta Cryst.* **1963**, *16*, 762. [[CrossRef](#)]
20. Naderi, H.R.; Nadri, P.; Sorouri, A.M.; Ganjali, M.R.; Ehrlich, H.; Nasrabadi, M.R.; Ahmadi, F. Evaluation of electrodes composed of europium tungstate/reduced graphene oxide nanocomposite for use as supercapacitors. *Surf. Interfaces* **2022**, *31*, 102002. [[CrossRef](#)]
21. Kodairaa, C.A.; Britoa, H.F.; Maltab, O.L.; Serrac, O.A. Luminescence and energy transfer of the europium (III) tungstate obtained via the Pechini method. *J. Lumin.* **2003**, *101*, 11–21. [[CrossRef](#)]
22. Karthikeyan, D.; Vijayakumar, K.; Suhasini, P.; Dhanusha, A.; Sabari, G.T.C. Third-order nonlinear optical responses of Cr³⁺ ions on La₂(WO₄)₃ nanoparticles for optical limiting applications. *J. Photochem. Photobiol. A Chem.* **2023**, *436*, 114377. [[CrossRef](#)]
23. Yun, F.; Cao, L.; Huang, J.; Wu, J. Effects of pH on the microstructures and optical property of FeWO₄ nanocrystallites prepared via hydrothermal method. *Ceram. Int.* **2013**, *39*, 4133–4138.
24. Kim, A.H.; Kang, J.H.; Hong, A.R.; Park, Y.J.; Jang, H.S.; Kang, Y.M.; Kim, D.H. Sputter-grown Eu-doped WO₃-Eu₂(WO₄)₃ composite red phosphor thin films. *Opt. Mater.* **2021**, *122*, 111721. [[CrossRef](#)]
25. Kubendhiran, S.; Sakthinathan, S.; Chen, S.M.; Lee, C.M.; Lou, B.S.; Sireesha, P.; Su, C. Electrochemically activated screen printed carbon electrode decorated with nickel nano particles for the detection of glucose in human serum and human urine sample. *Int. J. Electrochem. Sci.* **2016**, *11*, 7934–7946. [[CrossRef](#)]
26. Rajakumaran, R.; Babulal, S.M.; Chen, S.M.; Sukanya, R.; Karthik, R.; Shafi, P.M.; Shim, J.J.; Shiuan, C.Y. Ingenious design of iron vanadate engulfed 3D porous reduced graphene oxide nanocomposites as a reliable electrocatalyst for the selective amperometric determination of furaltadone in aquatic environments. *Appl. Surf. Sci.* **2021**, *569*, 151046. [[CrossRef](#)]
27. Horne, E.; Cadogan, A.; Keeffe, M.O.; Boom, L.A.P.H. Analysis of Protein-bound metabolites of Furazolidone and furaltadone in pig liver by high-performance liquid chromatography and liquid chromatography–mass spectrometry. *Analyst* **1996**, *121*, 1463–1468. [[CrossRef](#)]
28. Yan, C.; Teng, J.; Liu, F.; Yao, B.; Xu, Z.; Yao, L.; Chen, W. Signal amplified enzyme-linked immunosorbent assay with gold nanoparticles for sensitive detection of trace furaltadone metabolite. *Microchem. J.* **2020**, *159*, 105414. [[CrossRef](#)]

29. Barbosa, J.; Freitas, A.; Mourao, J.L.; Silveira, M.I.N.; Ramos, F. Determination of furaltadone and nifursol residues in poultry eggs by liquid chromatography-electrospray ionization tandem mass spectrometry. *J. Agric. Food Chem.* **2012**, *60*, 4227–4234. [[CrossRef](#)]
30. Bock, C.; Gowik, P.; Stachel, C. Matrix-comprehensive in-house validation and robustness check of a confirmatory method for the determination of four nitrofurans metabolites in poultry muscle and shrimp by LC-MS/MS. *Biomed Life Sci.* **2007**, *856*, 178–189. [[CrossRef](#)]

Disclaimer/Publisher's Note: The statements, opinions and data contained in all publications are solely those of the individual author(s) and contributor(s) and not of MDPI and/or the editor(s). MDPI and/or the editor(s) disclaim responsibility for any injury to people or property resulting from any ideas, methods, instructions or products referred to in the content.